Proceedings of the
Annual Stability Conference
Structural Stability Research Council
Atlanta, Georgia, April 21-24, 2026

A geometrically exact beam element for tapered I-section members

Rodrigo Gonçalves[1]

Abstract
A two-node beam finite element for thin-walled web- and flange-tapered I-section members is proposed in this paper. The element is based on the geometrically exact concept, meaning that the underlying formulation is independent of the magnitude of the displacements and rotations involved. 3D behavior is allowed, together with eccentric load effects, torsion-related warping and Wagner effects. All expressions required to implement the proposed finite element are provided in a simple matrix-vector format. A set of numerical tests is presented, to provide evidence of the accuracy and computational efficiency of the proposed element in linear, linear stability (calculation of bifurcation loads and buckling modes) and large displacement analyses. For comparison purposes, results taken from the literature, as well as refined shell finite element model solutions, are presented.

1. Introduction

Tapered I-section members are aesthetically appealing and structurally efficient, but their behavior is significantly more complex than their prismatic counterparts. For this reason, advanced structural analysis frequently relies on shell finite element (FE) models, due to the widespread availability of such elements in commercial programs. However, shell FE models are computationally expensive and do not provide the structural insight typically conveyed by beam FEs, namely information regarding internal forces and moments, as well as section-wise strain parameters such as extension, bending/torsion curvature and torsion-warping. In fact, if cross-section local deformation is not significant, beam elements should be favored.

Tapered beam models are more intricate than their prismatic counterparts, since it is necessary consider the variation of the cross-section along the length, as well as the inclination of the stresses and strains in the flanges. Several such beam elements, namely for tapered I-sections, have been proposed in the past. Most of these research efforts target the calculation of bifurcation loads and, in some cases, they also examine the linear solutions for the torsion problem, since tapered geometries require special attention to this case (see e.g. Kitipornchai & Trahair 1972, Ronagh et al. 2000a, b, Andrade & Camotim 2005, Trahair 2014). Regarding large displacements, the available research is scarcer. Boissonnade and Maquoi (2002) presented a tapered I-section beam FE that, even though includes some assumptions, allows large displacements using a corotational

[1] Full Professor, CERIS and Universidade Nova de Lisboa, Portugal <rodrigo.goncalves@fct.unl.pt>

description. However, in the validation examples presented, the torsional rotations are quite small (below 6º). The beam element proposed by Mohri et al. (2015) allows large twist angles, but only small bending rotations.

The geometrically exact beam theory — proposed by Reissner (1972, 1973), for the 2D case, and Simo (1985) for the spatial case — relies on exact nonlinear kinematics, via centerline position and rigid cross-section finite rotations, to describe finite strains. Consequently, it is independent of the magnitude of the displacements and rotations involved. The geometrically exact concept was first applied to tapered members by the author in a series of papers concerning thin-walled rectangular sections (Gonçalves 2023a, 2023b, 2024a). In Gonçalves (2024b) this work was summarized and extended to tapered cruciform cross-sections, in which case the beam can be modeled using two walls with coinciding centroids, considering only secondary (through-thickness) torsion-warping.

The present paper extends the previous work to the more general case of tapered I-sections. Both flanges and web can be linearly tapered and allowance is made for 3D behavior, load eccentricity with respect to the centroid, torsion-related warping and Wagner effects. The formulation is implemented in a two-node beam FE, and its accuracy is shown in a set of numerical tests involving linear, linear stability (bifurcation loads and buckling modes) and large displacement analyses. For comparison purposes, results taken from the literature, as well as results obtained with refined shell FE models, are presented.

Concerning the notation, the prime indicates a derivative with respect to X_3, while derivatives with respect to X_1 and X_2 are represented by subscript commas, e.g. $f' = \mathrm{d}f/\mathrm{d}X_3$ and $f_{,1} = \mathrm{d}f/\mathrm{d}X_1$. A tilde $\widetilde{\boldsymbol{a}}$ indicates an anti-symmetric matrix whose axial vector is $\boldsymbol{a}$, $\mathbf{0}_{n\times m}$ is an $n \times m$ matrix of zeros, and $\mathbf{1}_n$ represents the $n \times n$ identity matrix. A virtual variation is indicated by δ, whereas Δ denotes an incremental-iterative variation.

2. A geometrically exact beam element for tapered I-sections

2.1 Kinematics, strain and equilibrium

As shown in Fig. 1, the beam is considered an assembly of three walls, and three configurations are defined for each one. The *reference* configuration is identical for all walls, with $X_2, X_3 \in [-1,1]$ and $X_1 \in [-t/2, t/2]$, where t is the wall thickness. The *initial* configuration for each wall is then mapped using

$$\boldsymbol{x}_0 = \boldsymbol{r}_0 + \boldsymbol{\Lambda}_0 \boldsymbol{l}_0, \tag{1}$$
$$\boldsymbol{l}_0 = \boldsymbol{L}_C + \boldsymbol{R}(X_1\boldsymbol{E}_1 + (1+\tau)X_2\boldsymbol{E}_2), \tag{2}$$

where $\boldsymbol{r}_0(X_3)$ is the position vector of the cross-section centroid G, $\boldsymbol{\Lambda}_0$ is the cross-section rotation tensor, assumed constant for each element, $\boldsymbol{L}_C$ is the position vector of the wall centroid C with respect to G (hence $\boldsymbol{L}_C = \mathbf{0}$ for the web, while for the flanges it depends on the web taper), $\boldsymbol{R}$ is the rotation tensor of the wall and $\tau(X_3)$ is the taper function, assumed linear in this paper. The cross-section rotation $\boldsymbol{\Lambda}_0$ is deemed constant for each element and no shearing occurs, hence $\boldsymbol{\Lambda}_0^T\boldsymbol{r}_0' = \varepsilon_0\boldsymbol{E}_3$, where $\varepsilon_0 = \|\boldsymbol{r}_0'\|$ is the axial stretch from the reference to the initial configurations. For the web one has $\boldsymbol{R} = \mathbf{1}_3$, while for the flanges $\boldsymbol{R} = \boldsymbol{R}_1\boldsymbol{R}_3$, a composition of two rotations

where $\boldsymbol{R}_3$ is a positive 90º rotation along $\boldsymbol{E}_3$ (note the position of point A in the reference and initial configurations) and $\boldsymbol{R}_1$ is a rotation along $\boldsymbol{E}_1$, dependent on the web taper function.

For the *current* configuration one uses

$$\boldsymbol{x} = \underbrace{\boldsymbol{r}_0 + \widehat{\boldsymbol{u}}}_{\boldsymbol{r}} + \underbrace{\widehat{\boldsymbol{\Lambda}}\boldsymbol{\Lambda}_0}_{\boldsymbol{\Lambda}} \underbrace{(\boldsymbol{l}_0 + \omega\hat{p}\boldsymbol{R}\boldsymbol{E}_3)}_{\boldsymbol{l}}, \tag{3}$$

where $\widehat{\boldsymbol{u}}(X_3)$ is the displacement of the cross-section centroid G, $\widehat{\boldsymbol{\Lambda}}(X_3)$ is the cross-section rotation tensor between the initial and current configurations, $\omega(X_1, X_2, X_3)$ is the torsion-related warping function (to be determined) and $\hat{p}(X_3)$ is an amplitude function. It should be noted that warping occurs along $\boldsymbol{R}\boldsymbol{E}_3$, hence is inclined with respect to the member axis (the line of G).

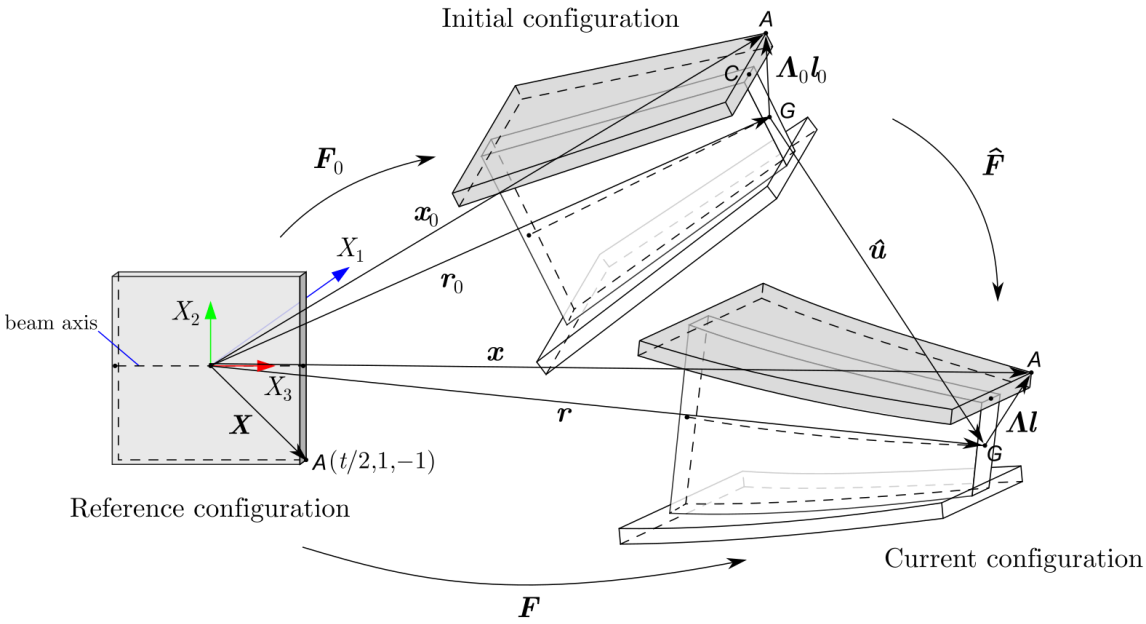

Figure 1: Reference, initial and current configurations of the tapered I-section beam

A back-rotated Green-Lagrange strain measure is used, reading

$$\begin{aligned} \widehat{\boldsymbol{E}} &= \tfrac{1}{2}\boldsymbol{\Lambda}_0^{\mathrm{T}}\left(\widehat{\boldsymbol{F}}^{\mathrm{T}}\widehat{\boldsymbol{F}} - \boldsymbol{1}\right)\boldsymbol{\Lambda}_0 = \tfrac{1}{2}\left(\textstyle\sum_{i,j=1}^{3}(\boldsymbol{g}_i \cdot \boldsymbol{g}_j)\boldsymbol{A}_{ij} - \boldsymbol{1}\right), \\ \boldsymbol{A}_{ij} &= \boldsymbol{G}_0^{-\mathrm{T}}\boldsymbol{E}_i \otimes \boldsymbol{E}_j\boldsymbol{G}_0^{-1}, \end{aligned} \tag{4}$$

with

$$\boldsymbol{F} = \frac{\mathrm{d}\boldsymbol{x}}{\mathrm{d}\boldsymbol{X}} = \boldsymbol{\Lambda}\boldsymbol{G}, \quad \boldsymbol{F}_0 = \frac{\mathrm{d}\boldsymbol{x}_0}{\mathrm{d}\boldsymbol{X}} = \boldsymbol{\Lambda}_0\boldsymbol{G}_0, \quad \widehat{\boldsymbol{F}} = \frac{\mathrm{d}\boldsymbol{x}}{\mathrm{d}\boldsymbol{x}_0} = \boldsymbol{F}\boldsymbol{F}_0^{-1}, \tag{5}$$

$$\boldsymbol{G}_0 = \textstyle\sum_{i=1}^{3}\boldsymbol{g}_{0i} \otimes \boldsymbol{E}_i, \quad \boldsymbol{G}_0^{-1} = \begin{bmatrix} 1 & 0 & -G_{13}^0/G_{33}^0 \\ 0 & 1/G_{22}^0 & -G_{23}^0/G_{22}^0G_{33}^0 \\ 0 & 0 & 1/G_{33}^0 \end{bmatrix}, \tag{6}$$

$$G_{22}^0 = 1 + \tau, \; G_{j3}^0 = \boldsymbol{g}_{03} \cdot \boldsymbol{E}_j, \; \boldsymbol{G} = \textstyle\sum_{i=1}^{3}\boldsymbol{g}_i \otimes \boldsymbol{E}_i = \sum_{i=1}^{3}(\boldsymbol{g}_{0i} + \widehat{\boldsymbol{g}}_i) \otimes \boldsymbol{E}_i, \tag{7}$$

$$\begin{cases} \boldsymbol{g}_{01} = \boldsymbol{E}_1 \\ \boldsymbol{g}_{02} = G_{22}^0 \boldsymbol{E}_2 = (1+\tau)\boldsymbol{E}_2 \\ \boldsymbol{g}_{03} = \boldsymbol{\Gamma}_0 + \boldsymbol{E}_3 + \boldsymbol{R}^T \boldsymbol{L}_C' + \tau' X_2 \boldsymbol{E}_2 \end{cases} \quad \begin{cases} \widehat{\boldsymbol{g}}_1 = \omega_{,1} \hat{p} \boldsymbol{E}_3 \\ \widehat{\boldsymbol{g}}_2 = \omega_{,2} \hat{p} \boldsymbol{E}_3 \\ \widehat{\boldsymbol{g}}_3 = \widehat{\boldsymbol{\Gamma}} + \boldsymbol{R}^T \widetilde{\boldsymbol{K}} \boldsymbol{l}_0 + (\omega \hat{p}' + \omega' \hat{p}) \boldsymbol{E}_3 \end{cases} \tag{8}$$

where the extension-shearing strains $(\boldsymbol{\Gamma}_0, \boldsymbol{\Gamma}, \widehat{\boldsymbol{\Gamma}})$ and curvature $\widetilde{\boldsymbol{K}}$ measures are given by

$$\begin{cases} \boldsymbol{\Gamma}_0 = (\boldsymbol{\Lambda}_0 \boldsymbol{R})^T \boldsymbol{r}_0' - \boldsymbol{E}_3 = \boldsymbol{R}^T \varepsilon_0 \boldsymbol{E}_3 - \boldsymbol{E}_3 \\ \boldsymbol{\Gamma} = (\boldsymbol{\Lambda} \boldsymbol{R})^T \boldsymbol{r}' - \boldsymbol{E}_3 \\ \widehat{\boldsymbol{\Gamma}} = \boldsymbol{\Gamma} - \boldsymbol{\Gamma}_0 \\ \widetilde{\boldsymbol{K}} = \boldsymbol{\Lambda}^T \boldsymbol{\Lambda}' = \boldsymbol{\Lambda}_0^T \widehat{\boldsymbol{\Lambda}} \widehat{\boldsymbol{\Lambda}}' \boldsymbol{\Lambda}_0 \end{cases} \tag{9}$$

The calculation of the strains requires the development of

$$\boldsymbol{g}_i \cdot \boldsymbol{g}_j = \boldsymbol{g}_{0i} \cdot \boldsymbol{g}_{0j} + \boldsymbol{g}_{0i} \cdot \widehat{\boldsymbol{g}}_j + \widehat{\boldsymbol{g}}_i \cdot \boldsymbol{g}_{0j} + \underline{\widehat{\boldsymbol{g}}_i \cdot \widehat{\boldsymbol{g}}_j}, \tag{10}$$

but the nonlinear underlined term is only preserved for the calculation of the longitudinal strains (hence $i = j = 3$), to allow capturing Wagner effects. After some algebra, it can be shown that the only non-null strain components correspond to two shear strains and the longitudinal strain, reading

$$\begin{cases} \hat{E}_{13} = \frac{1}{2}\left(\omega_{,1}\hat{p} + \frac{\boldsymbol{E}_1 \cdot \widehat{\boldsymbol{g}}_3}{G_{33}^0}\right) \\ \hat{E}_{23} = \frac{1}{2}\left(\frac{\omega_{,2}\hat{p}}{G_{22}^0} + \frac{\boldsymbol{E}_2 \cdot \widehat{\boldsymbol{g}}_3}{G_{33}^0}\right) \\ \hat{E}_{33} = -\frac{G_{13}^0 \omega_{,1}\hat{p}}{G_{33}^0} - \frac{G_{23}^0 \omega_{,2}\hat{p}}{G_{22}^0 G_{33}^0} + \frac{\boldsymbol{E}_3 \cdot \widehat{\boldsymbol{g}}_3}{G_{33}^0} + \frac{\widehat{\boldsymbol{g}}_3 \cdot \widehat{\boldsymbol{g}}_3}{2\left(G_{33}^0\right)^2} \end{cases} \tag{11}$$

Since the beam is thin-walled, it can be assumed that the warping function is subdivided according to $\omega = \bar{\omega} + X_1 \psi$, where $\bar{\omega}$ is the mid-line or membrane component, and ψ is the through-thickness or secondary component. These components can be obtained from the Kirchhoff constraint ($\hat{E}_{13} = 0$) and the Vlasov constraint ($\hat{E}_{23}(X_1 = 0) = 0$) for uniform torsion, leading to

$$\omega = \frac{G_{22}^0}{G_{33}^0} X_2 (-L_{C2} + \cos\beta \, X_1), \tag{12}$$

where L_{C2} is the X_2 component of $\boldsymbol{L}_C$ for the particular wall under consideration, and β is the rotation angle pertaining to $\boldsymbol{R}_1$. Note that the warping function depends on X_3 even if G_{22}^0, G_{33}^0 are constant, due to L_{C2}.

For a standard Saint Venant-Kirchhoff material law, the second Piola-Kirchhoff stresses $\widehat{\boldsymbol{S}}$ are related to the strains according to $\widehat{\boldsymbol{S}} = \boldsymbol{C}\widehat{\boldsymbol{E}}$, with

$$\widehat{\boldsymbol{S}} = \begin{bmatrix} \hat{S}_{33} \\ \hat{S}_{13} \\ \hat{S}_{23} \end{bmatrix}, \quad \widehat{\boldsymbol{E}} = \begin{bmatrix} \hat{E}_{33} \\ 2\hat{E}_{13} \\ 2\hat{E}_{23} \end{bmatrix}, \quad \boldsymbol{C} = \begin{bmatrix} E & 0 & 0 \\ 0 & G & 0 \\ 0 & 0 & G \end{bmatrix}, \tag{13}$$

where E is Young's modulus and G is the shear modulus. Then, from the virtual work statement, the equilibrium equations read

$$\delta W = -\int_V \delta \widehat{\boldsymbol{E}}^{\mathrm{T}}\, \widehat{\boldsymbol{S}}\, J_0 \mathrm{d}V + \delta \boldsymbol{x} \cdot \boldsymbol{Q} = 0, \tag{14}$$

where V is the beam volume at the reference configuration, $J_0 = \det(\boldsymbol{F}_0) = \det(\boldsymbol{G}_0) = G_{22}^0 G_{33}^0$, $\boldsymbol{Q}$ is a concentrated force (considered here instead of more general loads for simplicity purposes) and $\delta \boldsymbol{x}$ is the virtual variation of the work-conjugate position vector.

2.2 The finite element

A two-node beam FE is obtained by interpolating the nodal values of the displacement $\widehat{\boldsymbol{u}}$, the weight of the warping function $\hat{p}$ and the rotation vector $\widehat{\boldsymbol{\theta}}$ using linear functions. The latter vector is employed to parametrize the rotation tensor $\widehat{\boldsymbol{\Lambda}}$, thus allowing additive updates and a straightforward geometric interpretation of rotations (Cardona & Géradin 1988, Ritto-Corrêa & Camotim 2002, Peres et al. 2010). The element therefore has 7 DOFs per node and a total of 14 DOFs. The linear, linear stability and non-linear FE procedures were implemented in MATLAB (2024). For the non-linear case, the load-displacement path is traced using displacement control at a single DOF.

With one Gauss point integration along X_3, to avoid locking, the element stiffness matrix and internal force vector read

$$\begin{aligned}
\boldsymbol{K}_e &= \sum_{walls=1}^{3} \begin{bmatrix} \mathbf{1}_7 & \mathbf{1}_7 \\ -\mathbf{1}_7 & \mathbf{1}_7 \end{bmatrix}^T \int_{-1}^{1} \int_{-t/2}^{t/2} \left(\boldsymbol{\Xi}_{D\widehat{\boldsymbol{E}}}^T \boldsymbol{C} \boldsymbol{\Xi}_{D\widehat{\boldsymbol{E}}} + \boldsymbol{\Xi}_{D^2\widehat{\boldsymbol{E}}}\left(\widehat{\boldsymbol{S}}\right) \right) J_0 \, \mathrm{d}X_1 \mathrm{d}X_2 \,, \\
\boldsymbol{F}_e &= \sum_{walls=1}^{3} \begin{bmatrix} \mathbf{1}_7 & \mathbf{1}_7 \\ -\mathbf{1}_7 & \mathbf{1}_7 \end{bmatrix}^T \int_{-1}^{1} \int_{-t/2}^{t/2} \boldsymbol{\Xi}_{D\widehat{\boldsymbol{E}}}^T \widehat{\boldsymbol{S}}\, J_0 \mathrm{d}X_1 \mathrm{d}X_2 \,,
\end{aligned} \tag{15}$$

with the auxiliary matrices

$$\begin{aligned}
\boldsymbol{\Xi}_{D\widehat{\boldsymbol{E}}} &= \boldsymbol{\mathcal{G}}_0 \begin{bmatrix} \boldsymbol{\Xi}_{\omega,1} \\ \boldsymbol{\Xi}_{\omega,2} \\ \boldsymbol{\Xi}_{D\hat{g}_3} \\ 2\widehat{\boldsymbol{g}}_3^T \boldsymbol{\Xi}_{D\widehat{\boldsymbol{g}}_3} \end{bmatrix}, \\
\boldsymbol{\mathcal{G}}_0 &= \begin{bmatrix} -\frac{G_{13}^0}{G_{33}^0} & -\frac{G_{23}^0}{G_{22}^0 G_{33}^0} & 0 & 0 & \frac{1}{G_{33}^0} & \frac{1}{2\left(G_{33}^0\right)^2} \\ 1 & 0 & \frac{1}{G_{33}^0} & 0 & 0 & 0 \\ 0 & \frac{1}{G_{22}^0} & 0 & \frac{1}{G_{33}^0} & 0 & 0 \end{bmatrix}, \\
\boldsymbol{\Xi}_{\omega,1} &= [\mathbf{0}_{1\times3} \quad \mathbf{0}_{1\times3} \quad \omega_{,1} \quad \mathbf{0}_{1\times3} \quad \mathbf{0}_{1\times3} \quad 0], \\
\boldsymbol{\Xi}_{\omega,2} &= [\mathbf{0}_{1\times3} \quad \mathbf{0}_{1\times3} \quad \omega_{,2} \quad \mathbf{0}_{1\times3} \quad \mathbf{0}_{1\times3} \quad 0], \\
\boldsymbol{\Xi}_{D\widehat{\boldsymbol{g}}_3} &= \left[\mathbf{0}_{3\times3} \quad \boldsymbol{R}^T \begin{pmatrix} \boldsymbol{\Lambda}_0^T \boldsymbol{\Xi}_{D\widehat{\boldsymbol{\Lambda}}^T}(\boldsymbol{r}') \\ -\widetilde{\boldsymbol{l}}_0 \boldsymbol{\Lambda}_0^T \boldsymbol{\Xi}_{D\widehat{\boldsymbol{T}}^T}\left(\widehat{\boldsymbol{\theta}}'\right) \end{pmatrix} \quad \omega' \boldsymbol{E}_3 \quad \boldsymbol{R}^T \boldsymbol{\Lambda}^T \quad -\boldsymbol{R}^T \widetilde{\boldsymbol{l}}_0 \boldsymbol{\Lambda}_0^T \widehat{\boldsymbol{T}}^T \quad \omega \boldsymbol{E}_3 \right],
\end{aligned} \tag{16}$$

$$\boldsymbol{\Xi}_{D^2\widehat{\boldsymbol{E}}}(\widehat{\boldsymbol{S}}) = \boldsymbol{\Xi}_{D^2\widehat{\boldsymbol{g}}_3} + 2\mathcal{B}_6\boldsymbol{\Xi}^T_{D\widehat{\boldsymbol{g}}_3}\boldsymbol{\Xi}_{D\widehat{\boldsymbol{g}}_3},$$

$$\boldsymbol{\Xi}_{D^2\widehat{\boldsymbol{g}}_3} = \begin{bmatrix} \mathbf{0}_{3\times3} & \mathbf{0}_{3\times3} & \mathbf{0}_{3\times1} & \mathbf{0}_{3\times3} & \mathbf{0}_{3\times3} & \mathbf{0}_{3\times1} \\ & \begin{pmatrix}\boldsymbol{\Xi}_{D^2\widehat{\boldsymbol{\Lambda}}}(\boldsymbol{\mathcal{D}},\boldsymbol{r}') \\ +\boldsymbol{\Xi}_{D^2\widehat{\boldsymbol{T}}}(\boldsymbol{\mathcal{E}},\widehat{\boldsymbol{\theta}}')\end{pmatrix} & \mathbf{0}_{3\times1} & \boldsymbol{\Xi}^T_{D\widehat{\boldsymbol{\Lambda}}}(\boldsymbol{\mathcal{D}}) & \boldsymbol{\Xi}^T_{D\widehat{\boldsymbol{T}}}(\boldsymbol{\mathcal{E}}) & \mathbf{0}_{3\times1} \\ & & 0 & \mathbf{0}_{1\times3} & \mathbf{0}_{1\times3} & 0 \\ & & & \mathbf{0}_{3\times3} & \mathbf{0}_{3\times3} & \mathbf{0}_{3\times1} \\ & & & & \mathbf{0}_{3\times3} & \mathbf{0}_{3\times1} \\ \text{Sym.} & & & & & 0 \end{bmatrix}, \tag{17}$$

$$\boldsymbol{\mathcal{B}} = \widehat{\boldsymbol{S}}^T\boldsymbol{\mathcal{G}}_0,\ \boldsymbol{\mathcal{C}} = \begin{bmatrix}\mathcal{B}_3 \\ \mathcal{B}_4 \\ \mathcal{B}_5\end{bmatrix} + 2\mathcal{B}_6\widehat{\boldsymbol{g}}_3,\ \boldsymbol{\mathcal{D}} = \boldsymbol{\Lambda}_0\boldsymbol{R}\boldsymbol{\mathcal{C}},\ \boldsymbol{\mathcal{E}} = \boldsymbol{\Lambda}_0\widetilde{\boldsymbol{l}}_0\boldsymbol{R}\boldsymbol{\mathcal{C}},$$

where the auxiliary matrices $\boldsymbol{\Xi}_{D\widehat{\boldsymbol{\Lambda}}^T}$, $\boldsymbol{\Xi}_{D\widehat{\boldsymbol{T}}^T}$, $\boldsymbol{\Xi}_{D^2\widehat{\boldsymbol{\Lambda}}}$ and $\boldsymbol{\Xi}_{D^2\widehat{\boldsymbol{T}}}$ depend on the rotation vector and are given by Ritto-Corrêa and Camotim (2002).

3 Numerical examples

A series of illustrative numerical examples is presented next, to show the accuracy of the proposed beam FE. For comparison purposes, reference solutions are provided, taken from the literature and/or obtained using refined MITC4 shell FE models, using ADINA (Bathe 2022). The differences with respect to the reference solutions are calculated using $e = (d_{beam} - d_{ref})/d_{ref}$, where d_{beam} is the solution obtained with the proposed element and d_{ref} is the reference solution. All examples concern cantilevered beams with warping prevented at the fixed end, since in this case the boundary conditions are easily modeled using shell FEs. The cantilevers are subjected to forces and moments applied at the free end.

3.1 Linear analysis

A set of linear analyses are first carried out. Fig. 2 concerns a web- and flange-tapered cantilever subjected to free end 1 kN forces acting along each one of the global axes, causing bending or axial extension. The figure displays the beam geometry and material parameters, the deformed configurations for the proposed beam FE, as well as the displacement of the loaded point obtained with the proposed element and refined shell element models, showing an excellent match (differences below 1.5 %). It should be noted that the beam results shown were obtained with 15 equal length elements mainly to enhance the visualization of the deformed configurations, since less elements can provide equally accurate results (for instance five elements suffice for the force along X_1 case).

Fig. 3 concerns a standard benchmark example taken from the literature that assesses, for cantilevers subjected to a free end torque, the torque-free end rotation relation (T/ϕ) as a function of the web taper parameter α. The graph shows this relation, calculated with the proposed beam element (15 equal length elements) and provided by other beam elements from the literature (Kitipornchai & Trahair 1972, Ronagh et al. 2000b, Andrade 2005). Clearly, all solutions virtually overlap. It should be noted that, as a consequence of the inclination of the flanges, the minimum value occurs for $\alpha \approx 0.4$, rather than for the minimum α.

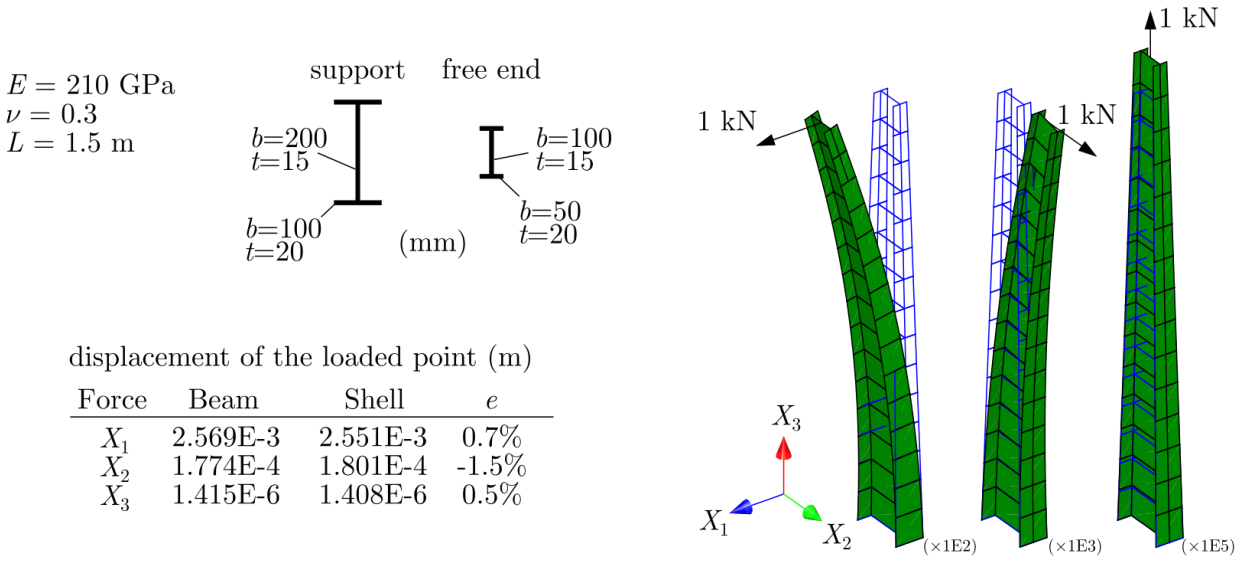

displacement of the loaded point (m)

Force	Beam	Shell	e
X_1	2.569E-3	2.551E-3	0.7%
X_2	1.774E-4	1.801E-4	-1.5%
X_3	1.415E-6	1.408E-6	0.5%

Figure 2: Linear analysis of a cantilever subjected to free end forces

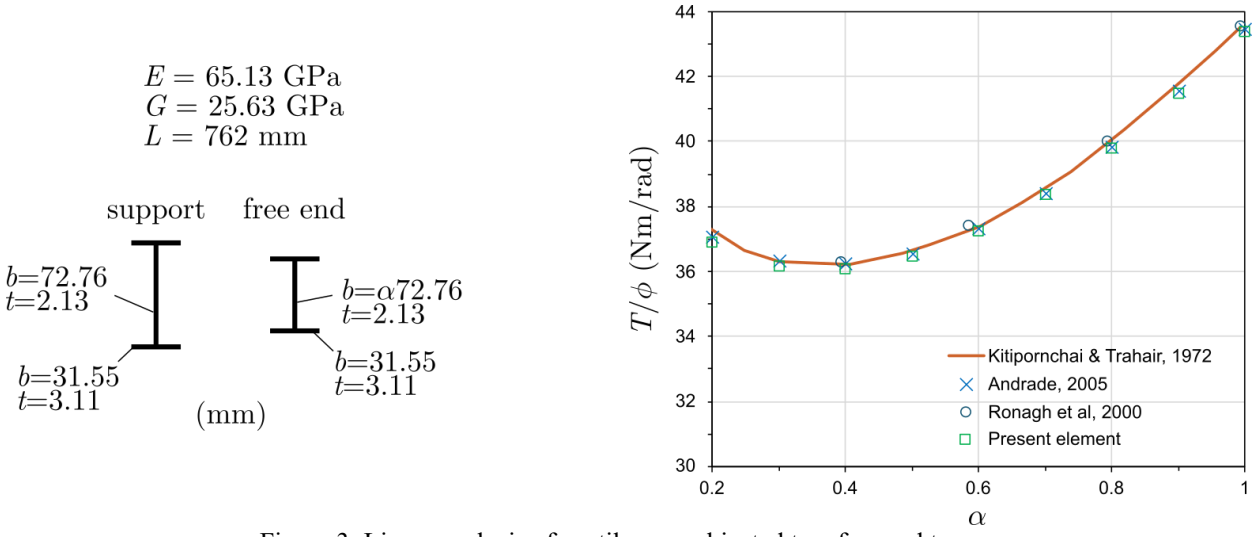

Figure 3: Linear analysis of cantilevers subjected to a free end torque

3.2 Linear stability analysis

Another benchmark example is reported in Fig. 4, in this case concerning a cantilever subjected to end forces acting along X_2, which trigger lateral-torsional buckling. The figure shows the problem geometry, the critical buckling modes obtained with the proposed beam FE (15 equal length elements), for top flange, centroid and bottom flange loading, as well as the normalized critical bifurcation loads $P_{cr}L^2/\sqrt{EI_2GJ}$ (with EI_2GJ calculated at the fixed end), obtained by Ronagh et al. (2000b), Andrade (2005), the present beam FE and refined shell FE models. When the loads are applied at the centroid of the flanges, the tangent stiffness matrix must include the term

$$\Delta\delta\boldsymbol{x}\cdot\boldsymbol{Q}=\Delta\widehat{\boldsymbol{\theta}}\cdot\boldsymbol{\Xi}_{D^2\widehat{\boldsymbol{\Lambda}}}(\boldsymbol{\Lambda}_0\boldsymbol{L}_C,\boldsymbol{Q})\delta\widehat{\boldsymbol{\theta}}, \tag{18}$$

which reflects the work of the external force $\boldsymbol{Q}$ when the cross-section rotates. A very close match between all models is observed, being worth noting that the proposed model is the closest to the shell FE solution, with differences $e \leq 2.4$ %. Note also that top/bottom flange loading have a destabilizing/stabilizing effect, respectively, with respect to centroid loading. The buckling modes are slightly different, with top flange loading leading to a higher twist of the free end cross-section.

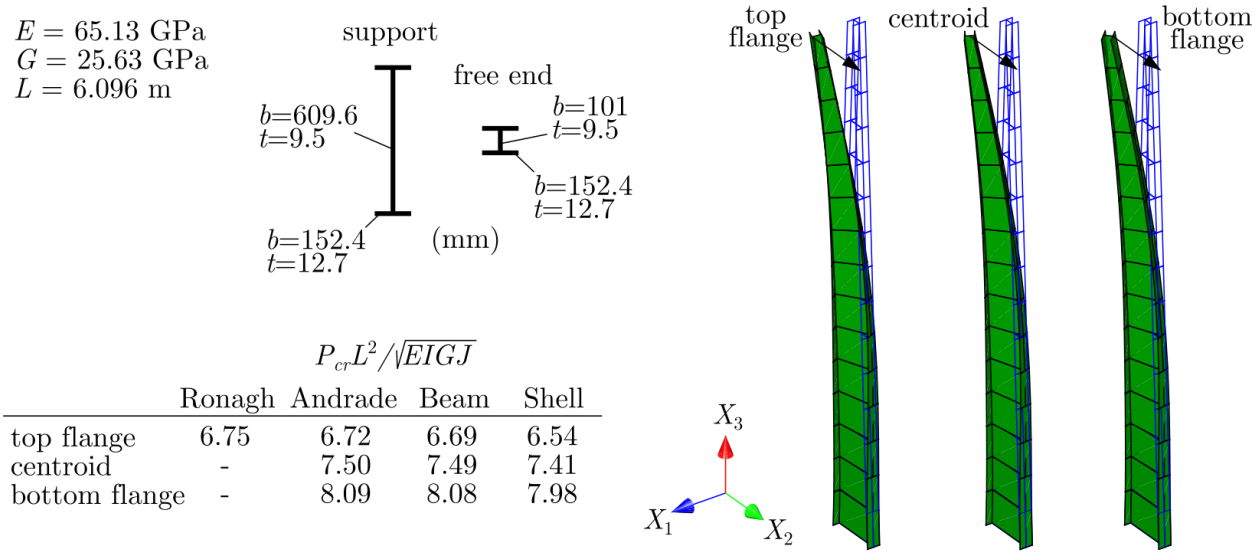

$P_{cr}L^2/\sqrt{EIGJ}$

	Ronagh	Andrade	Beam	Shell
top flange	6.75	6.72	6.69	6.54
centroid	-	7.50	7.49	7.41
bottom flange	-	8.09	8.08	7.98

Figure 4: Linear stability analysis of a cantilever beam subjected to a free end force along X_2

3.3 Large 3D displacements

Finally, an example concerning large spatial displacements and rotations is presented in Fig. 5. The load equals $\lambda \times 1$ kN, where λ is the loading parameter, and is applied at the centroid of the free end cross-section, at 45º along X_1 and X_2, causing biaxial bending and torsion. The graph shows the evolution of the loaded point displacement components with λ, obtained with the proposed beam model (15 FE) and a refined shell model (7670 FE). An excellent match is observed for all displacement components up to the onset of flange local buckling, which occurs for $\lambda \approx 260$, as shown by the wavy patterns in the detail of the shell model deformed configuration.

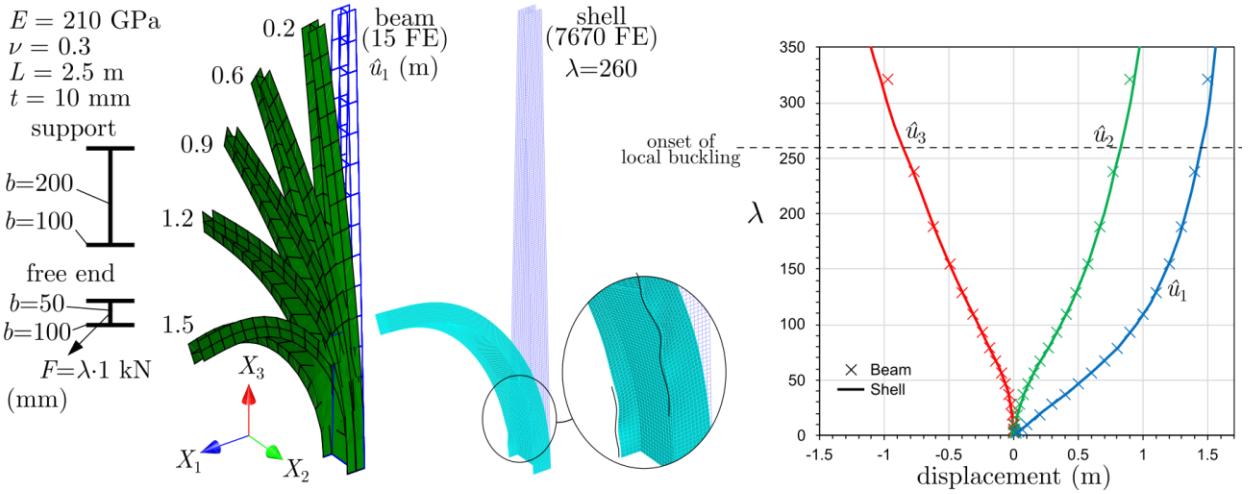

Figure 5: Nonlinear analysis of a cantilever beam subjected to a 45º end force

4. Conclusions

This paper proposed a geometrically exact 7 DOF two-node beam FE for thin-walled web- and flange-tapered I-section members. The element can handle large 3D displacements and rotations, eccentric loads and torsion-related warping. A close-form solution for the warping function was derived based on the Kirchhoff and Vlasov assumptions. Even though the underlying mathematics are quite involved, simple expressions are provided in the paper to facilitate the FE implementation. Several numerical examples were presented, to show the accuracy and computational efficiency of the element in linear, linear stability (calculation of bifurcation loads and buckling modes) and path-following large displacement analyses. In all cases a virtually perfect match with reference solutions was found, with the latter either taken from the literature or obtained using refined meshes of standard shell FEs.

One final remark to mention that the author is currently working on extending the present formulation in order to be able to include arbitrary warping functions and more general cross-section deformation.

Acknowledgments

This research was funded in whole or in part by the Fundação para a Ciência e a Tecnologia, I.P. (FCT, https://ror.org/00snfqn58) under Grant UID/6438/2025 (https://doi.org/10.54499/UID/06438 /2025) of the research unit CERIS. For the purpose of Open Access, the author has applied a CC-BY public copyright license to any Author's Accepted Manuscript (AAM) version arising from this submission.

References

Andrade, A., (2005). "Lateral Stability of tapered beams", MSc Thesis, Lisbon Technical University (in Portuguese).

Andrade, A., Camotim, D. (2005). "Lateral-torsional buckling of singly symmetric tapered beams: Theory and applications." *Journal of Engineering Mechanics*, 131(6), 586-597.

Bathe, K. J. (2022). *ADINA System*, ADINA R&D Inc.

Boissonnade, N., Maquoi, R. (2005). "A Geometrically and Materially Non-linear 3-D Beam Finite Element for the Analysis of Tapered Steel Members." *Steel Structures*, 5, 413-419.

Cardona, A., Géradin, M. (1988). "A beam finite element non-linear theory with finite rotations." *International Journal for Numerical Methods in Engineering*, 26, 2403-2438.

Peres, N., Gonçalves, R., Camotim D. (2021). "A geometrically exact beam finite element for curved thin-walled bars with deformable cross-section", Computer Methods in Applied Mechanics and Engineering, 31, 113804.

Gonçalves, R. (2023a). "A geometrically exact beam finite element for non-prismatic strip beams: The 2D case." *International Journal of Structural Stability and Dynamics*, 23(4), 2350037.

Gonçalves, R. (2023b). "A geometrically exact beam finite element for non-prismatic strip beams: Linearized lateral-torsional stability." *International Journal of Structural Stability and Dynamics*, 23(12), 2350139.

Gonçalves, R. (2024a). "A geometrically exact beam finite element for non-prismatic strip beams: The spatial case." *International Journal of Structural Stability and Dynamics*, available on-line, 245013823.

Gonçalves, R. (2024b). "A beam finite element for tapered and curved members." *Proceedings of the Annual Stability Conference Structural Stability Research Council, SSRC 2024*.

Kitipornchai, S., Trahair N. S. (1972). "Elastic stability of tapered I-beams." *Journal of the Structural Division*, 98(3), 713-728.

MATLAB, version R2024b, The MathWorks Inc., Massachusetts, 2024.

Mohri, F., Meftah, S., Damil, N. (2015). "A large torsion beam finite element model for tapered thin-walled open cross sections beams." *Engineering Structures*, 99, 132-148.

Reissner, E. (1972). "On one-dimensional finite-strain beam theory: the plane problem." *Z. Angew. Math. Phys.*, 23(5), 795-804.

Reissner, E. (1973). “On one-dimensional large-displacement finite-strain beam theory.” *Studies in Applied Mathematics*, 52, 87-95.

Ritto-Corrêa, M., Camotim, D. (2002). “On the differentiation of the Rodrigues formula and its significance for the vector-like parameterization of Reissner-Simo beam theory.” *International Journal for Numerical Methods in Engineering*, 55, 1005-1032.

Ronagh, H., Bradford, M., Attard, M. (2000a). “Nonlinear analysis of thin-walled members of variable cross-section. Part I: Theory.” Computers & Structures, 77(3), 285-299.

Ronagh, H., Bradford, M., Attard, M. (2000b). “Nonlinear analysis of thin-walled members of variable cross-section. Part II: Application.” Computers & Structures, 77(3), 301-313.

Simo, J. (1985) “A finite strain beam formulation. The three-dimensional dynamic problem. Part I.” *Computer Methods in Applied Mechanics and Engineering*, 49(1), 55-70.

Trahair, N. (2014). “Bending and buckling of tapered steel beam structures.” *Engineering Structures*, 59, 229-237.